Monitoring of Historical Glacier Recession in Yulong Mountain by the Integration of Multisource Remote Sensing Data

Linwei Yue, Huanfeng Shen, *Senior Member, IEEE*, Wei Yu, and Liangpei Zhang, *Senior Member, IEEE*

***Abstract*—Yulong Mountain, which is the southernmost snow-capped mountain in mainland Eurasia, has been confronted with significant glacier recession in the last decades due to global climate warming. The recession of these small-scale monsoonal temperate glaciers is a sensitive indicator of global warming. However, there have been few studies that have comprehensively monitored the historical glacier recession in Yulong Mountain area. This paper integrates multisource remote sensing data to monitor the glacial status on Yulong Mountain between 1957 and 2009. Integrating a topographic map, the long-term observed Landsat TM/ETM+ images, and multitemporal digital elevation model datasets, both the area change and regional mass balance of the Yulong glaciers are analyzed. According to the results, the area of the Yulong glaciers decreased from 11.57 to 4.55 km^2 at a rate of -0.14 km^2 yr^{-1} over the last 52 years between 1957 and 2009. The 1987–1999 specific mass balance was -0.31 ± 0.33 m yr^{-1} water equivalent, while the 1987–2008 mass balance was -0.27 ± 0.35 m yr^{-1} water equivalent. It can be interpreted from the results that the Yulong glaciers have experienced persistent glacier recession during the last decades. The glacier melting is still significant due to the continuously rising temperature. Furthermore, spatially heterogeneous glacier recession has been observed in this area. The glacier changes are spatially varied, which is probably due to the local temperature and precipitation, the glacier sizes, the terminus altitudes, and terrain factors. The influencing elements interacted with each other, and the climate conditions are the dominant factors affecting glacier status.**

***Index Terms*—Glacier change, monsoonal temperate glacier, multisource data fusion, remote sensing, Yulong Mountain.**

Manuscript received July 17, 2017; revised October 11, 2017; accepted November 11, 2017. Date of publication February 9, 2018; date of current version February 12, 2018. This work was supported in part by the Fundamental Research Funds for the Central Universities, China University of Geosciences, Wuhan (CUG170663), in part by the National Natural Science Foundation of China under Grant 41422108, and in part by the National Natural Science Foundation of China under Grant 41401383. *(Corresponding author: Huanfeng Shen.)*

L. Yue is with the Faculty of Information Engineering, China University of Geosciences, Wuhan 430074, China (e-mail: yuelw@cug. edu.cn).

H. Shen is with the School of Resources and Environmental Sciences and Remote Sensing and the Collaborative Innovation Center for Geospatial Technology, Wuhan University, Wuhan 430079, China (e-mail: shenhf@whu.edu.cn).

W. Yu is with the AutoNavi Software Ltd., Alibaba Group, Beijing 100102, China (e-mail: kyle.yw@alibaba-inc.com).

L. Zhang is with the State Key Laboratory of Information Engineering in Surveying, Mapping and Remote Sensing and the Collaborative Innovation Center for Geospatial Technology, Wuhan University, Wuhan 430079, China (e-mail: zlp62@whu.edu.cn).

This paper has supplementary downloadable material available at http://ieeexplore.ieee.org. The figures show the DEM coregistration and correction results, including the relationship between elevation differences and terrain factors before and after planimetric and vertial adjustment, and the elevation differences between SRTM1 and SRTM-X for the penetration estimation. The file is 0.203 MB.

Color versions of one or more of the figures in this paper are available online at http://ieeexplore.ieee.org.

Digital Object Identifier 10.1109/JSTARS.2017.2776901

I. Introduction

GLACIER changes, especially the changes of mountain glaciers, are one of the most sensitive indicators of terrestrial climate change [1]. Meltwater discharge from mountain glaciers is a significant water source for arid and semiarid areas. Meanwhile, the dramatic glacier fluctuation increases the risk of geological and flood disasters. In addition, glaciers feature fascinating geological landscapes, which are valuable presents from nature [2]. Therefore, the monitoring of glacial changes has been the subject of much research interest [1], [3]–[10].

Yulong Mountain, located in southwestern China at the southeastern edge of the Tibetan Plateau, is the southernmost snow-capped mountain in mainland Eurasia [11]. Thus, the status of the Yulong glaciers can be considered to be a representative indicator of global warming. This area is influenced by the westerly circulation and the southwest Indian monsoon, and is warm and moist in summer. According to the records, 70% of the total precipitation is concentrated in the warm season [11]. The glaciers in Yulong Mountain area are divided into four glacial basins: the Yanggong River basin, the Baishui River basin, the Daju Valley basin, and the Ren River basin (shown in Fig. 1). The meltwater of the glaciers in the Yanggong River basin flows into the Lijiang basin, while the melt runoff of the Baishui River glaciers and Daju Valley glaciers runs into Jinsha River.

Researchers have paid close attention to these small-scale monsoonal temperate glaciers. In the 1950s, Ren *et al.* [12] first studied the contemporary glaciers and quaternary geomorphology in Yulong Mountain. In the 2000s, He *et al.* [11], [13], [14] integrated climatic data and ice core records, and used modern environmental research methods to analyze the dynamics of the Yulong glaciers and the monsoonal temperate glaciers in China. They pointed out that the Yulong glaciers have retreated substantially over the last decades, and the glacier recession in Yulong Mountain can be mainly attributed to climate warming [15]. Local research works into Yulong Mountain have mainly concentrated on Baishui Glacier No. 1, the largest existing glacier on the eastern slope of the main peak [16], [17]. Pang *et al.* [18] reported the accelerating glacier retreat of Baishui Glacier No. 1 during 1998–2004. Li *et al.* [19] studied the snowpit

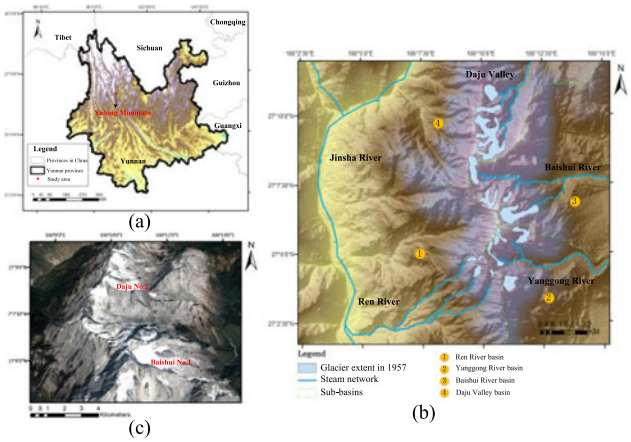

Fig. 1. (a) Geographical location of Yulong Mountain, Yunnan, China. (b) Distribution of the glaciers, main streams, and the division of the subbasins in the study area. (c) Three-dimensional view of Yulong Mountain, where the true-color image was obtained from Google Earth, acquired on November 22, 2015. The two largest individual glaciers, i.e., Baishui Glacier No. 1 and Daju Glacier No. 2, are labeled in (c).

chemistry on Baishui Glacier No. 1 using the samples collected in 2006. With the development of remote sensing techniques since the 1960s, they have become an effective way to monitor the dynamics of inaccessible mountain glaciers in rugged topography [20], [21]. Song [22] utilized glacier inventory data and remote sensing images to obtain the area shrinkage of the Yulong glaciers for 1957–1999. Du *et al.* [23] reported that the total area of glaciers in Yulong Mountain decreased from 11.61 km^2 in 1957 to 4.42 km^2 in 2009, based on field observations and remote sensing data. Moreover, Baishui Glacier No. 1 has been reported to have experienced dramatic melting in recent years [24]. Li *et al.* [10] studied the changes of climate, glaciers, and runoff during the last few decades in China's monsoonal temperate glacier areas, including Baishui Glacier No. 1 in Yulong Mountain. They reported the ablation rate at Baishui Glacier No. 1 to be -0.22 m yr^{-1} water equivalent (w.e.) during 1952–2004. However, the uncertainties of the results were not discussed, and the heterogeneous pattern of glacier fluctuations in Yulong Mountain was not examined.

The previous studies have been constrained by either using local field measurements or insufficient remote sensing data. Thus, there have been few studies that comprehensively monitored and analyzed the historical glacier recession in Yulong Mountain. Remote sensing is an efficient tool for the comprehensive monitoring of glaciers, and can provide us with large-scale multispectral and multitemporal observation data. Over the years, there have been numerous remote sensing-based studies of glacier cover mapping and volume change estimation [3], [25]–[29]. However, the degradation factors caused by the imaging mode and processing methods have limited the application feasibility.

Optical images are suitable for mapping glacier extent, due to the difference in the spectral reflectance of snow and ice between the visible and near-infrared (VNIR) band and the shortwave infrared (SWIR) band [30]. Nevertheless, the potential of optical images can be influenced by the spatial and temporal discontinuity. First, optical images are easily contaminated with cloud and haze, especially in humid mountainous regions, which prevents the images from being used for glacier information extraction [31]. Second, the image quality can be influenced by image noise and dead pixels during the generation process [32], [33]. For example, the Landsat satellite series have provided abundant multispectral terrestrial observations since 1972, which have been widely used in glacier mapping applications [6], [30]. However, the images are contaminated with dead stripes due to the failure of the scan line corrector (SLC) of the ETM+ sensor onboard Landsat-7 since 2003, which limits their application [34].

The accurate mapping of glacier extent with satellite images is also a challenging task. Generally speaking, clean ice/snow can be easily extracted using the remarkable spectral differences between the VNIR and SWIR bands (e.g., TM4/TM5). However, the glacier mapping results are usually affected by mountain shadow and debris cover on the ice. Many glacier mapping methods have been proposed, and most of them have focused on more accurate mapping of debris-covered glaciers by incorporating auxiliary information from the thermal band and digital elevation models (DEMs) [25], [28], [35], [36]. Overall, the present automatic methods are still not satisfactory for mapping glaciers, as a result of the difficulty of selecting the multiple thresholds. Thus, semiautomated methods have become popular in glacial applications, with automatic delineation of glaciers and manual postprocessing edits [6], [30], [35].

In addition to glacier area changes, multitemporal DEMs provide us with the opportunity to use the geodetic ice-to-mass method to obtain the glacier mass balance [37], [38]. However, the bias between the multisource DEMs can lead to a biased estimation of glacier mass balance. For example, the Shuttle Radar Topographic Mission (SRTM) elevation was found to be significantly underestimated in high-altitude areas [39]. If we use the SRTM DEM to estimate glacier mass loss, then the mass loss will be overestimated. Therefore, the systematic errors should be fully examined and corrected before computing the elevation changes [40], [41]. The horizontal and vertical biases of DEM data have been discussed in the previous works [3], [9],[40]. Nuth and Kaab [40] proposed a coregistration framework to obtain the analytical solution of the shifts between DEMs using the curve fitting of the elevation difference residuals and the terrain slope and aspect. For the vertical bias, the elevation-dependent bias is usually corrected by fitting a polynomial to the elevation differences on stable terrain [3]. Furthermore, the C-band penetration into snow and ice when using the SRTM DEM should also be considered [27], [41], [42].

In this study, we integrated multisource remote sensing data to monitor the glacier recession in Yulong Mountain from the mid-20th century to the early 21st century. Data fusion techniques for remote sensing data recovery and coregistration were employed, thereby improving the application accuracy with the full use of the complementary spatial and temporal information among the data. First, a temporal series of Landsat images observed during 1989–2009 were selected to extract the glacier extent. For the missing stripes in the recent Landsat images, a multitemporal regression method was employed to recover the missing values with the temporal auxiliary information [34]. A semiautomated method was then used for the glacier extraction,

TABLE I
LANDSAT IMAGES USED FOR THE GLACIER AREA MAPPING

	1	2	3	4
Date	22/08/1989	05/09/1994	15/08/2001	24/10/2009
ID number	LT51310411989234BKT00	LT51310411994248BJC00	LE71310412001227SGS00	LE71310412009997SGS00
Sensor	Landsat 5 TM	Landsat 5 TM	Landsat 7 ETM+	Landsat 7 ETM+
Cloud cover	13%	23%	13%	4%

considering the influence of cloud cover and terrain shadow. Combined with the glacier extent digitized from the historical topographic map produced in 1957, the glacier area changes for 1957–2009 could be obtained. The results in our study were basically consistent with the results obtained by Du *et al*. [23], which will be further discussed in Section VI. In terms of the glacier mass loss, three DEM datasets acquired at different times were used to calculate the glacier elevation changes and mass balance of Yulong Mountain for 1987–2008. The DEMs were coregistered and corrected in terms of the horizontal shift and vertical systematic biases to obtain more reliable results. After the correction, the mean elevation changes were converted to mass balance and the uncertainties were estimated. Finally, seasonality correction for the two February DEMs was considered to obtain the full-year mass balance [3], [27].

The main objective of this study was to fully investigate and fuse the complementary information within the multisource and multitemporal remote sensing data, and give a comprehensive analysis of the glacier changes in Yulong Mountain. With the estimated glacier area extent and mass balance results, the glacier recession status in Yulong Mountain area between 1957 and 2009 was analyzed. In addition, the response pattern of the glaciers to global warming and the spatially heterogeneous glacier changes were investigated.

Section II gives a detailed description of the data employed in the study. In Section III, we present the methods used in the process of extracting the glacier information and the uncertainty analysis. The results and discussions are then given in Sections IV and V. Finally, Section VI provides our conclusion.

II. DATA

A. Historical Glacier Map

The First Glacier Inventory Dataset of China (1956–1983) and the Second Glacier Inventory Dataset of China Version 1.0 (2006–2010) provided the glacier codes, locations, and other attribute parameters, which were used as the reference and guide to choose the remote sensing images for glacier extraction [43]. Moreover, a 1:50000 paper topographic photo obtained by aerial photogrammetry in 1957 was used to extract the glacier extent in Yulong Mountain. This map had a coordinate system of the Beijing 1954 and 1956 Yellow Sea height datum of China.

B. Landsat TM/ETM + Images

Landsat images were employed to extract the changing glacier extent during the last decades. The images that were cloud-free over the glaciers and with minimal snow cover were considered suitable for glacier mapping [25]. The images for glacier mapping were generally acquired at the end of summer, and there was no seasonal snow in the scenes. However, many of the images taken at the end of the summer ablation period are affected by large-area cloud cover, due to the moist climate conditions on Yulong Mountain in the warm season. Thus, it is difficult to obtain images suitable for glacier mapping. Between 1989 and 2009, four TM/ETM+ scenes were chosen to map the glacier area in this study, as listed in Table I and shown in Fig. 2. Unfortunately, there were no suitable images after 2009 for glacier mapping, due to the snow conditions and cloud cover.

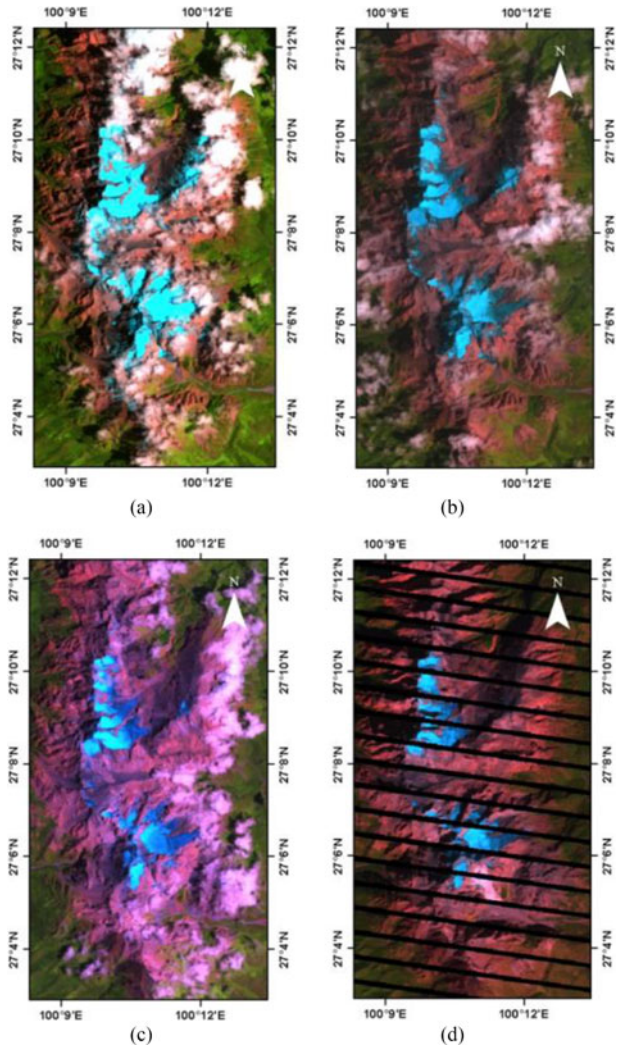

Fig. 2. Landsat images used for glacier mapping acquired on (a) August 22, 1989, (b) September 5, 1994, (c) August 15, 2001, and (d) October 10, 2009 (false-color composite of band 543).

As seen in Fig. 2, the ETM+ images acquired after 2003 were contaminated with dead stripes. The image scenes collected in this study were the L1T products after systematic radiometric and geometric correction. All the images were projected in Universal Transverse Mercator (UTM) zone 47N.

C. DEM Datasets

Three DEM datasets were employed to obtain the glacier elevation changes. The datasets were the 10-m contour map from 1987, and two raster DEMs generated from the February 2000 SRTM and Advanced Spaceborne Emission and Reflection radiometer (ASTER) stereo scenes acquired in February 2009.

The first DEM dataset was a 10-m contour map generated from aerial photogrammetry acquired in 1987 by the Chinese Yunnan Survey Service. The contour map had the coordinate system of Xi'an 1980 and geoid model of the 1985 Yellow Sea height datum of China.

The second DEM was the SRTM1 C-band data acquired in February 2000. This 11-day mission used radar interferometry to generate near-global data products of land elevation, covering over 80% of the Earth's surface $(60^\circ N - 56^\circ S)$ [45]. With two sensors on board with different electromagnetic spectra, the C-band and X-band observations were acquired simultaneously. The DLR SRTM-X DEMs have a spatial resolution of ∼25 m referenced to the WGS84 datum, but are limited in spatial coverage (with zonal gaps) [46]. Moreover, the SRTM-X DEMs were seriously affected by noises. Due to the wide spatial coverage and the specific acquisition time, the SRTM-C DEMs have been widely used in glacier change monitoring [4], [27], [47]. Unlike most of the previous works, we used the recently released 1 arc-second SRTM1 (∼30 m) DEM to replace the 3 arcsec SRTM3 (∼90 m) DEM product in our study. Compared with the SRTM3 data, the SRTM1 data have a higher spatial resolution and better vertical accuracy. Both of the DEMs were on the WGS84 horizontal datum and EGM96 vertical datum [48].

The third DEM dataset was the ASTER DEM generated by stereo images acquired in 2009. Two cloud-free L1A ASTER stereo images acquired on 17 February 2009 were used to automatically generate the ASTER DEM with a 30-m resolution. The DEM was georeferenced to the coordinate system of UTM 47N and geodetic datum of EGM96. Due to the influence of thick cloud and the limited spatial coverage of the satellite observations (e.g., Terra ASTER, TerraSAR), we did not include the data covering the small-scale snowcapped Yulong Mountain in the 2010s in this study. The status of the Yulong glaciers after 2009 was predicted and analyzed with the help of field investigation records [24].

D. Climate Data Records

The climate data recorded by the national weather station at Lijiang, located at ∼2381 m ($100^\circ 13' E$, $26^\circ 51' N$, ∼20 km away from Yulong Mountain), were used to analyze the glacier response to climate change. These data can be obtained from the China Meteorological Data Service Center (CMDC, http://data.cma.cn/). The monthly precipitation and monthly averaged air temperature for 1951–2015 were collected in this study. These data were also used to calculate the seasonality correction for the SRTM DEM and ASTER DEM collected in winter.

III. Methods

A. Datum Conversion and Resampling

First, the 1957 paper map needed to be digitized, and the 1987 contour map was converted to a raster DEM with a resolution of 12.5 m, corresponding to the contour interval. To be consistent with the Landsat images and DEM data, the historical map and 1987 DEM were then georeferenced to the WGS84/EGM96 datum. The datum conversion between different ellipsoidal systems was implemented with the seven-parameter method [49]. In addition, the ellipsoidal elevation of SRTM-X (h_{WGS84}) was converted to the orthometric elevation $H = h_{\mathrm{WGS84}} - N$, where N is the EGM96 geoid value [50]. All the data involved in the subsequent process were resampled to 30 m and georeferenced to WGS UTM 47N and the EGM96 geoid datum. Furthermore, orthorectification using the projected DEM was applied to all the remote sensing images, to limit the projection error related to the terrain effect.

B. Glacier Extraction

1) Recovering the Landsat SLC-Off Images: The dead stripes existing in the ETM+ SLC-off data degrade the data interpretation accuracy. One of the images we selected for the glacier mapping was contaminated with dead stripes, as shown in Fig. 2. In this study, the gap-filling algorithm proposed by Zeng *et al.* [34] was employed to recover the missing pixels for the Landsat ETM+ SLC-off images acquired on 24/10/2009. With the multitemporal SLC-off images, a weighted linear regression (WLR) algorithm can recover the missing pixels using the auxiliary information. The algorithm uses the information in the auxiliary image $\boldsymbol{x}$ to fill the missing pixels in the target image $\boldsymbol{y}$ with the linear relationship calculated from locally similar pixels, which can be expressed as follows:

$$y_t = a \cdot x_t + b \tag{1}$$

where x_t and y_t are the pixels at target location t in the image pair, and a, b are the regression coefficients. The coefficients can be obtained using the locally similar pixels in the multitemporal images selected based on the adaptive spatial similarity in each band. To search for similar pixels, the initial size of the local search window was defined as 7×7 pixels. If not enough pixels were obtained for the calculation, the size of the search window was expanded with a step length of two. The process ended after at least 30 similar pixels were chosen in the calculation of the coefficients. The weighted least-squares method was then employed to calculate the coefficients, with the expanded form as follows:

$$a = \frac{\sum_{i=1}^{n} W_i \left(y_i - \bar{y}\right)\left(x_i - \bar{x}\right)}{\sum_{i=1}^{n} W_i \left(x_i - \bar{x}\right)}, b = \bar{y} - a\bar{x} \tag{2}$$

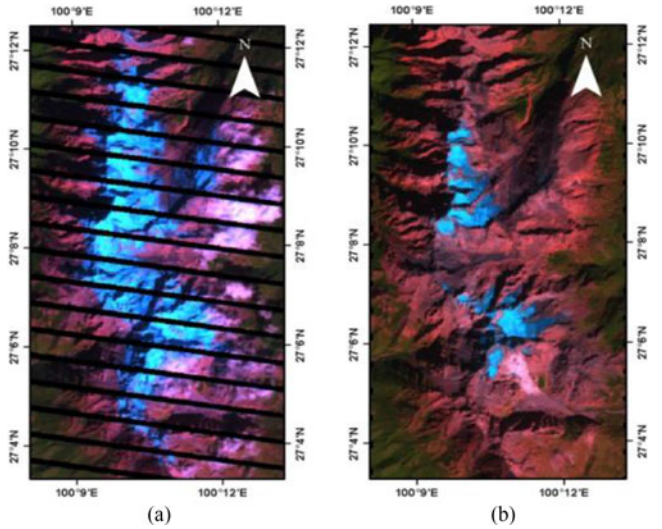

Fig. 3. Recovered SLC-off Landsat images obtained using the WLR algorithm. The Landsat data acquired on (a) October 30, 2011 were used to recover the image obtained on October 24, 2009, and the recovered image is shown in (b).

where $\bar{x}$ and $\bar{y}$ are the mean values of the similar pixels within the search window in the auxiliary and target image, respectively. The normalized weight W_i is assigned according to the spectral and spatial differences between the n selected similar pixels and the target pixel. More details of the algorithm can be found in the work of Zeng *et al.* [34].

The Landsat scene acquired on 30/10/2011 was used as the auxiliary data for the multitemporal recovery of the images. The results after gap filling are shown in Fig. 3. It can be seen that this method performs well in recovering the dead stripes in the ETM+ images.

2) Glacier Mapping: The long-term glacier extent for Yulong Mountain was extracted from the 1957 historical map and the multitemporal Landsat images listed in Table I. The glacier area in 1957 was extracted manually from the digitized map after datum conversion. For glacier mapping from the Landsat images, a multithreshold method was first used to roughly extract the ice extent. The clean ice was extracted using the high contrast in reflectivity between the VNIR and SWIR wavelengths, i.e., Band 4 and Band 5 for the TM/ETM+ images. Thus, the equation $B4/B5 > 2$ was used to distinguish the clean glacier ice from the nonglacier surface in this study. A threshold of 2 was selected empirically, and proved to be effective [25]. The glacial areas covered with supraglacial debris and mountain shadow can have a similar spectral reflectance to the nonglacier dark areas. Considering that the glaciers in the study area have limited debris cover, we incorporated the solar incident angle φ calculated with the DEM data and the band ratio to map the glaciers in the shadow regions. The thresholds for the incident angle and band ratio were set as follows:

$$(B4/B5 > 1.5) \text{ and } (\cos(\varphi) < 0.5). \tag{3}$$

The automatically extracted glaciers were generated integrating the results from the clean ice and the glaciers in the shadow areas. Manual postprocessing was then conducted to adjust the glacier outlines and remove the misclassified areas affected by water surfaces and cloud. As cloud is common in mountainous regions, it is difficult to accurately map the glaciers obscured by thick cloud. We thus employed the temporally neighboring scenes and the glacier inventory data to assist with the mapping of the obscured glaciers. For example, the terminus of Baishui Glacier No. 1 is partially covered by cloud in the ETM+ image acquired on August 15, 2001. Therefore, the ETM+ image acquired on October 29 1999 (ID: LE71310411999302SGS00) was used as the auxiliary reference to estimate the terminus location. Moreover, the glacier inventories were also used as a reference to map the glaciers and separate the individual glaciers into different drainage basins.

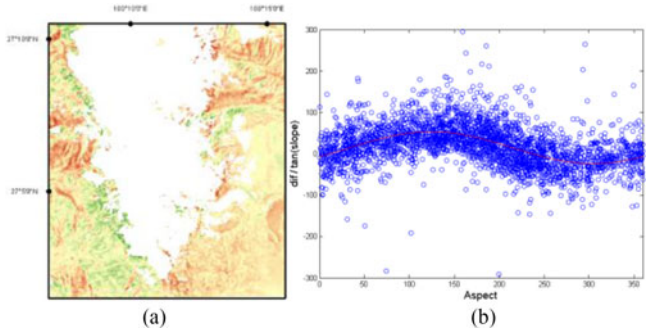

Fig. 4. Relationship between the elevation differences and terrain factors: (a) is the difference map between the SRTM1 2000 DEM and the 1987 DEM over stable terrain, while (b) is the scatter plot of $dh/\tan(\text{slope})$ and the terrain aspect.

C. Glacier Mass Balance

1) DEM Coeegistration and Correction: The systematic biases among the multisource DEMs were corrected in four steps: horizontal shift; elevation-dependent bias; curvature-dependent bias; and snow/ice penetration. Considering the original spatial resolution and the vertical accuracy, the DEM generated from the 1987 contour map (hereafter referred to as the 1987 DEM) was chosen as the reference data. The SRTM1 2000 DEM and ASTER 2009 DEM were coregistered and corrected based on the reference. To minimize the influence of glacier elevation changes, all the elevation differences were computed on the stable areas, with glacier/water pixels and anomalies excluded.

First, the horizontal shift was corrected using the relationship between the elevation differences and terrain aspect. It can be seen from Fig. 4 that the elevation differences are closely related to the terrain effect. In Fig. 4(b), the scatter plots of $dh/\tan(\text{slope})$ and the terrain aspect can be observed to fit the shape of a cosine function.

The analytical model proposed by Nuth and Kaab [40] was used to implement the coregistration, which can be expressed as follows:

$$dh = a \cdot \cos(b - \psi) \cdot \tan(\alpha) + dh_m \tag{4}$$

where dh is the elevation difference, while a and b are the magnitude and direction of the shift. α and ψ represent the terrain slope and aspect, while dh_m is the mean elevation bias between the two DEMs. Slope and aspect are computed with the reference DEM. The parameters a, b, and dh_m are solved using least-squares minimization. After acquiring the estimated

parameters, the corrected shift along the x-direction (along the longitude) is $a \cdot \sin(b)$, while the y-direction (along the latitude) shift and the mean vertical bias correction are $a \cdot \cos(b)$ and dh_m, respectively.

After coregistration, the vertical bias is corrected using the statistical relationship between the elevation differences and terrain factors. Generally speaking, the elevation-dependent bias and the curvature-dependent bias are considered to have a polynomial relationship [3], [40]:

$$dh = \mu_n Z^n + \tau \tag{5}$$

where Z is the elevation or maximum curvature, μ and τ are the regression parameters, and n is the order of the polynomial, which is selected from one to five in most cases. In this study, we used the cubic polynomial to simulate the elevation-dependent bias and performed linear regression for the curvature-dependent bias correction.

In addition to the above error terms, the bias caused by the snow/ice penetration of the radar C-band needed to be removed using the SRTM1 2000 DEM. The penetration can reach up to 9 m in the areas covered with dry snow in Greenland, and decreases with higher moisture [27]. Considering the same acquisition time and the negligible penetration of the X-band wavelength, the SRTM-X data were used to correct the C-band radar penetration [9], [41]. The SRTM-X data were coregistered to the corrected SRTM1 2000 DEM, and the elevation-dependent and curvature-dependent bias between the X- and C-band data were then corrected following the method described before. Finally, the penetration was estimated by comparing the elevation difference between the two datasets over glacier/snow areas.

2) Mass Balance Estimation: The glacier mass balance was computed using the three DEM datasets, i.e., the 1987 DEM, the 2000 SRTM1 DEM, and the 2009 ASTER DEM, after coregistration and correction. For the glacier mass balance calculation, the glacier extent extracted from 1989 was used to approximate the glacier area in 1987. The area change from 1987 to 1989 over a two-year period was slight compared with the long-term glacier retreat.

Pixels with absolute elevation differences larger than 100 m or pixels within the voids in the SRTM data were initially abandoned. Anomalies were then excluded if their absolute elevation differences exceeded $3\,\sigma$ at the corresponding altitude range. After excluding the anomalies, the elevation differences were averaged for each 100-m altitude range and considered as the approximate mean elevation change for the altitude. The density of ice was assumed to be 900 kg/m^3, to convert the average elevation changes into mass balance. The regional mass balance could then be calculated using the area-weighted average method [3], [8], [51]:

$$M_A = \frac{\sum_1^n M_r \cdot S_r}{\sum_1^n S_r} \tag{6}$$

where M_r is the mass balance at the $r\mathrm{th}$ altitude, and S_r is the area.

The aerial photogrammetry derived elevation data were acquired in the warm season (the specific acquisition time is unknown), while the DEMs used in our study were acquired in February (winter in the northern hemisphere). Thus, the seasonal accumulation need to be considered. In this study, the total precipitation from October to February recorded at Lijiang Station was computed and considered as the approximate seasonal accumulation. This was subtracted from the estimated mass to obtain the final result. Although this estimation was only approximate, it had little impact on the long-term annual mean value. Due to the lack of data, we did not investigate the spatial variability of snow accumulation in this region [52], [53].

In this study, the mean equilibrium line altitude (ELA) estimated by the "Hess method" was used to distinguish the ablation and accumulation areas [54]. This method delineates the average ELA as the transition or inflection from a concave to convex contour, which is likely shaped by the different glacier motion characteristics due to the accumulation and ablation effects. The mass balance results for the ablation and accumulation areas are given in Section V.

D. Uncertainty Analysis

The uncertainties include the errors of the glacier area delineation and glacier mass balance. In this study, we used an automatic method to generate the glacier areas, and then manual editing was undertaken afterward to adjust the glacier boundaries by visual interpretation. For glacier mapping, the manual delineation method is generally considered to be more accurate [28]. The extracted area statistics obtained in this study are similar to the previous results [23]. Therefore, we regard the derived glacier inventory obtained in this study as the actual glacier extent.

The uncertainties for the regional mass balance include the error terms of the elevation change estimation $(E_{\Delta h})$, the SRTM penetration correction (E_{pene}), and the seasonality correction (E_{season}). The standard deviation of the elevation changes $\sigma_{\Delta h}$ was calculated with the standard deviation $\sigma_{\Delta \mathrm{hi}}$ of each altitude range. Considering the spatial autocorrelation of the DEM errors, the standard error of the mean was reduced with the spatially independent measurements N [55]:

$$E_{\Delta \mathrm{hi}} = \frac{\sigma_{\Delta \mathrm{hi}}}{\sqrt{N}}. \tag{7}$$

In this equation, $N = N_{\mathrm{tot}}/2d$, where N_{tot} is the total number of pixels used to calculate the mean elevation changes of the corresponding altitude range, and d is the distance of the spatial autocorrelation. A suitable value for d was found to be 600 m for a spatial resolution of 30 m (20 pixels) [5]. The standard error $E_{\Delta h}$ was then computed as the area-weighted sum of $E_{\Delta \mathrm{hi}}$ for the altitude ranges. In the case of using the SRTM1 data, the error of the SRTM penetration estimation was computed with the elevation differences between the SRTM X-band and SRTM C-band data in the same way as described above.

The climate data used in this study were recorded at Lijiang Station. However, it is possible that the local precipitation on the mountain might be very different from the station records. Moreover, the differences between precipitation and seasonal accumulation needed to be considered. As a result, in this study, the error of the seasonality correction was estimated as 100% of the accumulated mass [3]. Finally, the resulting uncertainty for

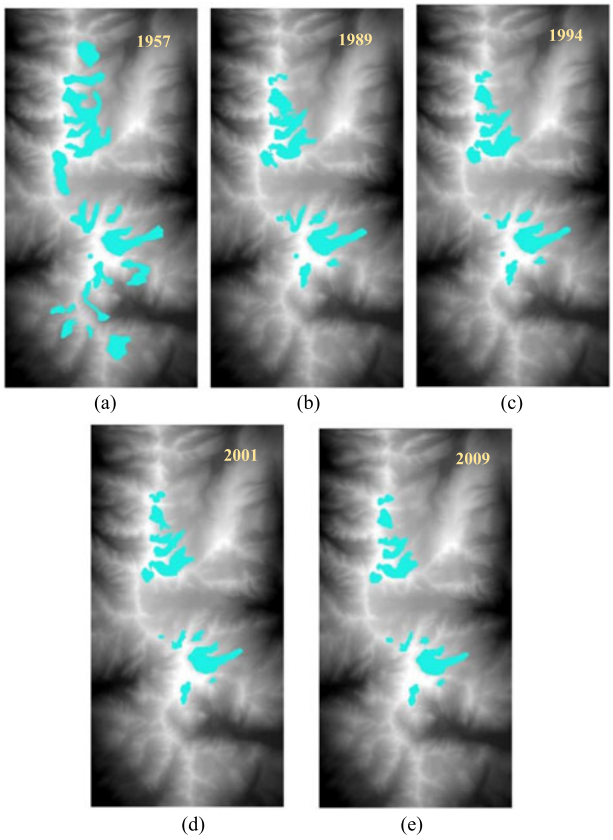

Fig. 5. Extracted glacier areas from 1957–2009.

the mass balance was obtained with the standard principles of error propagation [56]:

$$\sigma = \sqrt{\mathrm{MED}^2 + E_{\Delta h}^2 + E_{\mathrm{season}}^2 + E_{\mathrm{pene}}^2} \tag{8}$$

where MED is the mean elevation difference between the DEMs calculated over the off-glacier areas.

IV. Results and Analysis

A. Glacier Area Change During 1957–2009

The glacier areas of Yulong Mountain were derived from the historical inventory and remote sensing images from 1957–2009, as shown in Fig. 5, where significant glacier recession can be observed. In 1957, there were 19 glaciers with a total area of 11.57 km^2 in Yulong Mountain, based on the results obtained in our study. Seven glaciers disappeared over the last 52 years, and only 12 glaciers still existed in 2009 according to the remote sensing observations. The glaciers in Yulong Mountain lost 60.7% of their total area ($\sim$7.02 km^2). The remaining area of glaciers was 4.55 km^2 in 2009, and the decrease rate was $-0.14\,\mathrm{km}^2\,\mathrm{yr}^{-1}$ for 1957–2009.

The three-dimensional distribution of the glaciers and the temporal glacier extent changes are shown in Fig. 6. Among the glaciers, 15 are distributed on the eastern slope. The four glaciers in the Ren River basin on the western slope, with a total area of 0.73 km^2, had disappeared completely by 2009, according to the remote sensing images. It can also be observed from the figure that the glacier change is dramatic, with the

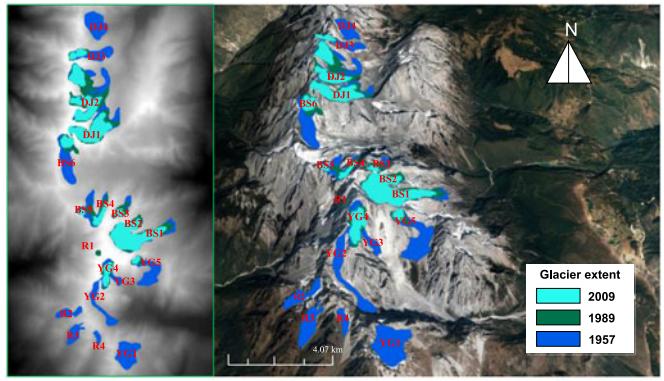

Fig. 6. Distribution of the glaciers and the extracted glacier area in Yulong Mountain during 1957–2009. The glaciers are divided into four basins: the Ren River basin (R), the Baishui River basin (BS), the Yanggong River basin (YG), and the Daju Valley basin (DJ).

glaciers showing large-scale recession, especially from 1957 to 1989. As a result of the glacier retreat, the terminus altitudes have increased sharply, along with the decrease of the glacier areas. Among the individual glaciers, the terminus altitude of Baishui Glacier No. 1 can be observed to rise from 4083 to 4295 m between 1957 and 2009, with an average increase rate of 4.1 $\mathrm{m\,yr}^{-1}$. During 1989–1994, the five-year average increase rate of the terminus altitude reached $12.8\,\mathrm{m\,yr}^{-1}$.

B. Glacier Mass Change During 1987–2008

1) DEM Correction Results: In Section III, we introduced the coregistration and correction method for the multiple DEM datasets involved in the glacier mass balance calculation [40], [41]. The SRTM1 2000 DEM and ASTER 2009 DEM were coregistered and corrected based on the high-accuracy 1987 DEM. In the following, the detailed correction results of SRTM1 are given as an example to prove the effectiveness of the correction process.

In our case, the $x-$ and $y-$ shifts to the SRTM1 DEM were $+1.08$ and -0.66 pixels, respectively. The subpixel coregistration process was implemented with the bilinear resampling algorithm. The relationship between $dh/\tan(\mathrm{slope})$ and the terrain aspect before and after the coregistration process was examined (see Fig. S1, in the Supporting Document). The trigonometric distribution of the elevation difference due to the horizontal errors between the DEMs was successfully eliminated.

After the planimetric registration, the vertical bias was then corrected using the relationship between the elevation difference and the elevation and terrain maximum curvature over the stable areas, considering the systematic vertical error and the errors caused by the resolution difference [40], [41]. The relationship between the elevation and the terrain factors before and after the vertical adjustment is shown in Fig. S2 (Supporting Document), where the elevation differences are the mean values calculated for each 100-m altitude interval. The elevation biases between the DEM datasets related to the terrain factors were effectively removed.

In addition, the quantitative evaluation results over the off-glacier terrain are given in Table II, where the stepwise correction results are shown. After the three-step correction, the

TABLE II
OFF-GLACIER QUANTITATIVE EVALUATION OF THESRTM1 BEFORE AND AFTER THE STEPWISE CORRECTION (UNIT: M)

	Original	Coregistration	Elev-dependent bias	Curve bias
MEAN	6.423	−2.260	0.248	−0.669
STD	21.693	16.862	14.996	14.544
MAX	71.751	58.437	52.041	49.702
MIN	−71.743	−58.432	−52.031	−49.731

TABLE III
OFF-GLACIER QUANTITATIVE EVALUATION OF THE ASTER DEM BEFORE AND AFTER THE STEPWISE CORRECTION (UNIT: M)

	Original	Coregistration	Elev-dependent bias	Curve bias
MEAN	7.263	8.120	2.714	−1.526
STD	34.609	32.840	31.423	30.868
MAX	121.095	116.178	111.731	110.154
MIN	−121.132	−116.175	−111.774	−110.157

vertical accuracy shows a significant improvement, with the mean error close to 0 and the standard deviation decreased, as shown in the fifth column in Tables II and III. All the results were calculated using the pixels with larger than three times the corresponding standard deviation excluded.

Similarly, the ASTER 2009 DEM was coregistered and corrected as described above. The quantitative correction results are given in Table III. The accuracy of the ASTER DEM is affected by noise, and thus it is less accurate than the SRTM1 DEM. However, the improvement is still promising after the correction.

In the case of using the SRTM1 DEM, the SRTM-X DEM is used as the auxiliary information to estimate the C-band radar penetration depth. The elevation difference of the SRTM1 and SRTM-X DEMs before and after correction is shown in Fig. S3 (Supporting Document). The elevation differences were calculated over the off-glacier, snow-covered, and glacier areas, respectively. There was an obvious underestimation of the X-band data over the off-glacier terrain without coregistration and correction, which prevented us from estimating the penetration height directly. Thus, the X-band data were coregistered and corrected to the corrected SRTM1 data following the method described in Section III. Based on the results calculated with the corrected datasets (see Fig. S3(b), Supporting Document), the mean C-band penetration depth was set as 1.5 m below 4800 m over the glacier areas, while the penetration reached ∼3.5 m above 4800 m with the lower temperature and moisture.

2) Glacier Mass Balance: The glacier mass balance in Yulong Mountain was calculated with the corrected DEM datasets, as described in Section III. The zones above 5400 m were not included in calculating the mass balance, because the area ratio of the altitude was too small. The percentage of the abandoned area was only 0.11%, which had little impact on the final estimation. The mean annual mass balance for 1987–2000 was obtained using the SRTM1 2000 DEM and the 1987 DEM. To show the effect of the correction process, we list the estimated 1987–2000 mass balance obtained using the stepwise corrected DEM dataset in Table IV. It can be seen that the vertical systematic bias has the most significant impact on the estimation, while the curvature-dependent bias has a relatively small influence on the final mass balance. The final estimated mean annual glacier mass balance is $-0.30\,\mathrm{m\,yr^{-1}}$ w.e. Compared with the original result, the correction of $+0.47\,\mathrm{m\,yr^{-1}}$ w.e. was added to the initial estimation. This is consistent with the conclusion in the work of Berthier *et al.* [39]. The mass loss was overestimated when using the SRTM DEM, due to its systematic bias. Similarly, the mean annual mass loss for 1987–2009 can be estimated as $-0.27\,\mathrm{m\,yr^{-1}}$ w.e., which was calculated with the 1987 DEM and the corrected ASTER DEM acquired in February 2009. In Fig. 7, the mean elevation changes and the area ratio of each altitude during the two periods are displayed. In the low-altitude glacier areas, the elevation changes are negative, due to glacier recession. The elevation changes of the two periods around 4100 m are generally equivalent, while the negative elevation change at the altitude zone above 4200 m during 1987–2009 is more significant than for 1987–2000. This might be caused by the long-term persistent glacier recession and the increase of the terminus altitudes.

The seasonality accumulation for the DEM data was finally corrected. Referring to the climate data records, the estimated mass accumulated from October 1999 to February 2000 was +0.15 m w.e., while the accumulated mass from October 2008 to February 2009 was estimated as +0.07 m w.e. Considering the overall estimated uncertainty, the final glacier mass balance for 1987–1999 was $-0.31 \pm 0.33\,\mathrm{m\,yr^{-1}}$ w.e., while the mass balance for 1987–2008 was $-0.27 \pm 0.35\,\mathrm{m\,yr^{-1}}$ w.e.

In our study, the results were obtained assuming the density of a glacier to be a fixed value of $900\,\mathrm{kg/m^3}$. Considering the different densities for snow/firn and pure ice, another common assumption is to apply the density as $900\,\mathrm{kg/\,m^3}$ in the ablation area and $600\,\mathrm{kg/\,m^3}$ in the firn zone [7]. Using the different densities above and below the firn line, the mass balance for 1987–1999 was calculated as $-0.29 \pm 0.28\,\mathrm{m\,yr^{-1}}$ w.e., while the mass balance for 1987–2009 was calculated as $-0.26 \pm 0.29\,\mathrm{m\,yr^{-1}}$ w.e. The results with the different density scenarios are comparable, and the values show similar trends to the results in the work of Kaab *et al.* [7]. The estimation with varying densities is dependent on the detection of the firn line (i.e., the equilibrium line for the temperate glaciers). In this paper, we give the results calculated with the different density scenarios to allow a comparison with other works. However, the analysis is mainly based on the results calculated with $900\,\mathrm{kg/\,m^3}$.

The estimated results obtained using the geodetic method were influenced by the glacier extent, to some extent, as given in (6). Therefore, the estimated mean mass loss rate for a long time period might be underestimated with the decreasing glacier area.

V. DISCUSSIONS

A. Glacier Changes and Climate Change

The status of glaciers is directly influenced by climate change, mainly referring to air temperature and precipitation [1]. There were no available long-term local meteorological data for the study area, and the scale of the available remote sensing data

TABLE IV
IMPACT OF THE STEPWISE CORRECTION ON THE MASS BALANCE ESTIMATION FOR 1987–2000

Unit: (m yr^{-1} w.e.)	Original	Coregistration	Elev-dependent bias correction	Curvature correction	Penetration correction
Mass balance	−0.77	−1.28	−0.35	−0.49	−0.30
Step-wise correction		−0.51	+0.93	−0.14	+0.19

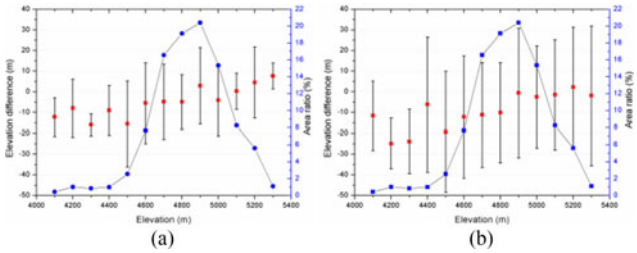

Fig. 7. Elevation difference as a function of altitude and the area ratio for the altitudes: (a) and (b) are the elevation differences for 1987–2000 and 1987–2009, respectively.

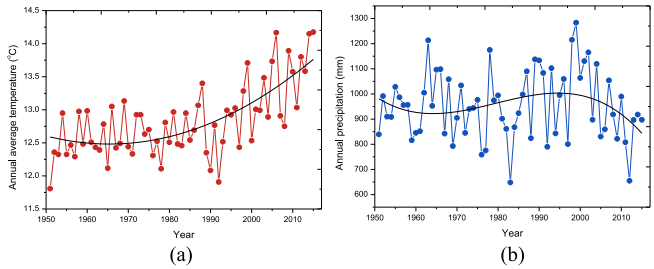

Fig. 8. Records of the annual average temperature and annual precipitation for Yulong Mountain, as provided by Lijiang Station: (a) and (b) indicate the fluctuations and fitting trends of the temperature and precipitation, respectively.

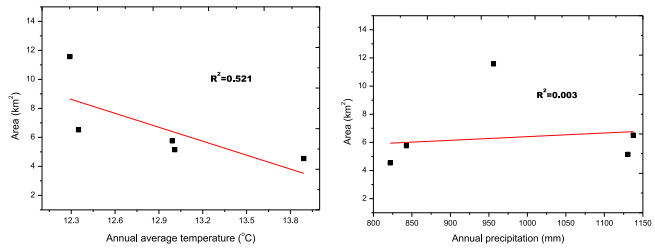

Fig. 9. Change curves of the glacier area shrinkage for 1957–2013.

(e.g., TRMM, GRACE) was too coarse for the study area. Therefore, we employed the climate records from Lijiang Station (shown in Fig. 1) for the analysis. As shown in Fig. 8, there has been an obvious increasing trend for the annual average temperature and increased fluctuation in the annual precipitation over the last decades from 1950. The correlation between the changes of the glaciers and climate data is given in Fig. 9. It can be seen in the figure that the correlation between glacier change and temperature is much higher than that for precipitation. The *R*-squared value between area change and annual average temperature reaches 0.521, while the correlation between area change and precipitation is only 0.003.

Temperatures in China's monsoonal temperate glacial region have been observed to have increased in a fluctuating manner over the last decades, and the temperature increase has accelerated since the 1980s [10], [57]–[59]. The data used in these analyses were the climate data from meteorological stations, ice core records, and the reconstructed results from tree-ring index studies. For the study region, the mean annual temperature at the elevation of ∼4600 m for Baishui Glacier No. 1 has shown a fluctuating upward trend since the 1950s, and the difference between the warmest decade and the coldest decade has reached 2.79 °C [60]. Based on all these facts, the glacier recession in Yulong area is mainly caused by the climate warming effect, while the precipitation is insufficient to compensate for the rapid ablation.

TABLE V
ESTIMATED MASS BALANCE FOR 1987–2008 (UNIT: M YR^{-1} W.E.)

	Ablation areas	Accumulation areas
1987–1999	-0.49 ± 0.32	-0.11 ± 0.33
1987–2008	-0.50 ± 0.30	-0.04 ± 0.36

The glaciers in Yulong Mountain have been sensitive to the warming climate, given that a sharp recession has been observed over the last decades, along with the increase of air temperature. As shown in Figs. 5 and 6 in Section IV, the area shrinkage has been dramatic from the mid-20th century, with seven glaciers disappearing by 2009. Although the remaining glaciers are of a larger size and have higher terminus altitudes, the retreat rate of the glaciers has remained at a high level from the end of the 20th century to recent years, without slowing down, which is likely due to the obviously rising trend of the temperature. Due to the lack of data, we do not give the monitoring results after 2009. However, the response pattern analyzed from the historical data can provide some clues. As the increase in temperature accelerated during the 2010s, and precipitation reduced dramatically in recent years (see Fig. 8), the glaciers in Yulong Mountain are probably retreating at an increasing rate.

B. *Spatially Heterogeneous Glacier Changes*

In addition to the temporal changes, it is also necessary to analyze the spatial variation in the rate of glacier changes. In terms of the glacier mass balance, the glacier status was monitored in both the accumulation and ablation areas, respectively. The average ELA in Yulong Mountain was roughly estimated as 4850 m using the Hess method, and the mass balance was then calculated in the accumulation and ablation areas within different periods, as shown in Table V. It can be seen that the glaciers retreated rapidly in the ablation areas, and the high-altitude glaciers experienced a slight negative balance, which resulted in the significant glacier mass loss from the mid-1980s [10].

TABLE VI
MASS BALANCE OF THE GLACIERS IN THE DIFFERENT BASINS AND THE GLACIER INFORMATION DERIVED FROM THE TM IMAGE ACQUIRED IN 1989 AND THE 1987 DEM (UNIT FOR MASS BALANCE: M YR^{-1} W.E.)

	Baishui No. 1	Baishui River basin	Daju No. 2	Daju Valley basin	Overall
1987–1999	-0.20 ± 0.34	$+0.03 \pm 0.22$	-0.88 ± 0.33	-0.52 ± 0.32	-0.31 ± 0.33
1987–2008	-0.24 ± 0.38	-0.07 ± 0.34	-0.55 ± 0.47	-0.41 ± 0.36	-0.27 ± 0.35
Area (km^2)	1.44	2.92	1.79	3.12	6.56
Average slope	20.85	22.93	24.66	22.82	24.38
Average aspect	84.15	117.24	77.06	84.45	106.28

Moreover, the spatially heterogenous changes of the glaciers in different subbasins were analyzed using the integrated glacial information. First, we give the change curves of glacier area shrinkage in Fig. 9. From the results, it can be seen that the glaciers in the Daju Valley basin have shown a relatively steady decrease, and the area shrinkage in the Baishui River basin has accelerated since the 1990s. The area loss of the glaciers in the Yanggong River basin was more prominent in the earlier decade.

The heterogeneous glacier changes caused by glacial (e.g., size and volume) and locational factors were investigated. In 1957, there were 16 glaciers in Yulong Mountain with an area smaller than $1\,\mathrm{km}^2$, referring to $\sim$60% of the total glacial area. Among these glaciers, seven vanished and 83.1% of the area was lost during 1957–2009. However, the three glaciers larger than $1\,\mathrm{km}^2$ (i.e., Baishui Glacier No. 1, Daju Glacier No. 1, and Daju Glacier No. 2) only lost 27.7% of the area. It can also be observed that the areas of the Yulong glaciers in the Ren River and Yanggong River basins have shown a more significant shrinkage than the northern glaciers over the last decades. Most of the glaciers in the Yanggong River and Ren River basins are located on the western slope, while the glaciers in the Baishui River and Daju Valley basins are mainly oriented to the north and east. It appears that the glacier size and location are directly related to the ablation rate. However, the small glaciers mainly occur in the low-altitude areas, and the terminus altitudes of the six vanished glaciers were all less than 4500 m. Furthermore, the main difference between the western and eastern slopes is the sunshine condition. The temperature is generally higher in the low-altitude and sunny-slope areas, which directly leads to the rapid recession of the glaciers.

The mass loss and the basic information of the glaciers distributed in the different basins are shown in Table VI. Excluding the data voids and anomalies, only the mass budgets of the glaciers in the Baishui River basin and Daju Valley basin could be obtained. It can be seen from the table that the glaciers located in different basins have behaved differently. The regional mass balance in the Baishui River basin was slightly negative at $-0.07 \pm 0.34\,\mathrm{m\,yr}^{-1}$ w.e. during 1987–2008. In contrast, the northern Daju Valley glaciers experienced relatively prominent ablation, with a mass loss rate of $-0.41 \pm 0.36\,\mathrm{m\,yr}^{-1}$ w.e. during 1987–2008. Furthermore, Daju Glacier No. 2 experienced a much faster mass loss rate than Baishui Glacier No. 1, which was consistent with the area change status. Baishui Glacier No. 1 and Daju Glacier No. 2 are of similar size, average slope, and aspect, and the terminus altitude of Baishui Glacier No. 1 is even lower than that of Daju Glacier No. 2. As the rainfall in Yulong Mountain is mainly brought by the southwest monsoon, the variation is probably caused by the precipitation difference between the two regions. Even within the same basin with similar climate conditions, the glacier changes have varied with different individual glaciers. In the Baishui River basin, Baishui Glacier No. 1 has retreated faster than the neighboring Baishui Glacier No. 2.

Based on the results, it can be inferred that the glacier recession was the synergistic consequence of multiple elements, including the temperature and precipitation, glacier size, the terminus altitude, and topographic factors. Instead of being independent, the influencing factors interact with each other. For example, the development of a glacier (e.g., size and volume) is dependent on the climate and terrain conditions, while the climate and terrain factors act on the glacier dynamics. In addition, the locational factors are indirectly related to the temperature and precipitation. Temperature is generally higher in the areas with lower altitude and more solar radiation, and precipitation varies with the terrain topology and underlying surface, as well as the altitude. Among the influencing elements, the climate conditions are the dominant factors affecting glacier status. At high altitudes, most of the precipitation falls as snow. Precipitation enables glacier accumulation, while higher temperature causes faster glacier ablation. However, alongside the increasing temperature in the region, the precipitation has played a weak role in the glacier changes, as shown in Fig. 10.

C. Comparison With Other Studies

In the work of Du *et al.* [23], it was reported that the glacier areas in Yulong Mountain decreased from 11.61 to 4.42 km^2 during 1957–2009. The glacier area in 2001 was estimated as $5.30\,\mathrm{km}^2$. In our work, the total glacier area in 1957 was calculated to be 11.57 km^2, while the areas in 2001 and 2009 were estimated to be 5.16 km^2 and 4.55 km^2, respectively. The inevitable errors might be caused by the data sources, the manual delineation, and the different calculation methods. However, the maximum difference is 2.7% when compared with Du's results, and the difference in 1957 is only 0.3%. Considering the different mapping methods employed, the results can be considered to be accurate.

There have been few studies that have comprehensively monitored the overall glacier mass balance of Yulong Mountain. However, the local studies of changes of Baishui Glacier No. 1 derived from reliable field investigation data can be used to validate the accuracy of the remote sensing results. As reported in [10], the mass balance in Baishui Glacier No. 1 was -11.38 m w.e. for 1952–2004, with an annual average of $-0.22\,\mathrm{m\,yr}^{-1}$

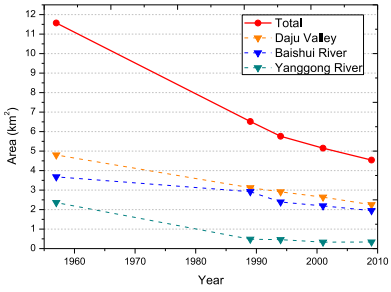

Fig. 10. Correlation between glacier changes and climate factors: (a) and (b) indicate the scatter plots between area and annual average temperature and annual precipitation, respectively.

w.e. over the past 52 years. According to the mass balance records, the glacier ablation was mainly concentrated around 1984 due to the significantly rising temperature and drought climate in this year. Recently, Du *et al.* [24] used the collected field measurements obtained during 2008–2013 to analyze the recession on Baishui Glacier No. 1. The results showed that the glacier mass showed a huge loss over the study period, with a mass balance of $-1.39\,\mathrm{m\,yr^{-1}}$ w.e.

According to the results obtained in this study, the mass balance of Baishui Glacier No. 1 was estimated as $-0.20 \pm 0.34\,\mathrm{m\,yr^{-1}}$ w.e. during 1987–1999 and $-0.24 \pm 0.38\,\mathrm{m\,yr^{-1}}$ w.e. during 1987–2008. An accelerating retreat rate of Baishui Glacier No. 1 from the end of the 20th century was reported in [18], which was confirmed in this study. It can be seen that the estimated results are in agreement with the historical records in [10]. However, the significant difference in the mass balance estimation for 1987–2009 and 2008–2013 should be examined. First, the long-term mean glacier mass balances of glaciers derived from the geodetic methods are probably underestimated. Furthermore, there has been a severe and enduring drought in southwestern China since 2010 [62]. It can be observed from the climate data shown in Fig. 10 that there was a fluctuation in temperature and precipitation in the 2000s. In contrast, the temperature kept rising and the precipitation remained at a low level from 2010 to 2015. Based on the climate conditions, the dramatic increase in loss rate is possible.

Similar trends can be found in the other studies of glacier mass balance estimation in China. Hailuogou Glacier, which is also a monsoonal glacier, located in Hengduan Mountains, was observed to have experienced an accelerated shrinkage from the mid-1980s. Along with the strong ablation, glacier holes, supraglacial streams, and crevasses were widely distributed on the glacier surface [10]. Compared with Hailuogou Glacier, Baishui Glacier No. 1 is smaller and located at a lower altitude. The annual average mass balance of Urumqi No. 1 Glacier located in Tien Shan was calculated as $-0.29\,\mathrm{m\,yr^{-1}}$ w.e. between 1959–2010, while the minimum glacier mass was estimated as -1.33 m w.e. in 2010 [61]. Moreover, the glacier mass balance of the high-altitude Puruogangri ice field on the Tibetan Plateau has been reported to have changed from $-0.04\,\mathrm{m\,yr^{-1}}$ w.e. between 2000–2012 to $-0.32\,\mathrm{m\,yr^{-1}}$ w.e. between 2000 and 2016 in recent years, with a much faster ablation rate [63], [64].

VI. Conclusion

In this study, we integrated the glacier area changes extracted from a historical map and Landsat TM/ETM+ images and the mass balance estimated from multisource elevation datasets to monitor the long-term recession of glaciers in Yulong Mountain. Multisource and multitemporal information was fully examined and utilized to improve the data availability and accuracy. From the results, the glacier recession was found to have been both significant and persistent in this area over the last decades, caused by climate warming.

The glacier retreat was analyzed from both the perspectives of area change and mass balance. With the long-term glacier recession, the remaining glaciers are now of larger sizes and/or located in areas with a higher altitude. However, the area change rate and the glacier mass balance results indicate that the mass loss rate is still persistent and significant, and glacier melting continues to accelerate in the Yulong area.

Spatially heterogeneous changes of glaciers were observed in Yulong Mountain. First, the mass balance in the accumulation areas was found to be slightly positive, while the mass loss in the ablation areas contributed to the overall negative mass budget. Moreover, the glacier changes varied between different individual glaciers. The spatially heterogeneous behavior of glacier changes was the synergistic consequence of multiple factors, including climate, glacial, and topographic factors. However, the increase of the annual average temperature and the insufficient precipitation supply were the main causes leading to the glacier ablation.

A comparison with other studies using field investigation and historical records was also undertaken. It was found that the results derived from remote sensing data are in agreement with the regional estimation by field investigation. Remote sensing can provide large-scale measurements, which is more suitable for monitoring large-scale glacial changes. The temporal inconsistency caused by cloud and the multisource spatial uncertainties are the main obstacles influencing the accuracy of remote sensing methods in glacial applications. In this study, we tried to solve some of the issues by data fusion; however, more studies are needed to minimize the uncertainties brought by the remote sensing data and methods. In this study, we did not address the altitudinal variation of precipitation or the impact of artificial snow augmentation in the analysis. In addition, under the influence of cloud cover, the use of optical satellite images does not work well. Thus, we did not use the changes of ELAs or the albedo retrieved from remote sensing images for further analysis in our study [65], [66].

Due to the resolution limit of the remote sensing data sources, it was difficult to include the influence of the terrain details (e.g., crevasses, subglacial holes) in the glacier mass balance in this study. With the development of remote sensing techniques, data with a higher resolution and quality might enable us to obtain more accurate results.

Acknowledgment

The authors gratefully thank Prof. Y. He, Dr. J. Du, and J.Liu from the State Key Laboratory of Cryosphere Science (Lijiang Station), Cold and Arid Regions Environmental and Engineering

Institute, Chinese Academy of Sciences, Lanzhou, China, for the great help in discussing the results and improving the manuscript. They also appreciate the editors and the anonymous reviewers for their valuable suggestions.

REFERENCES

[1] F. Paul *et al.*, "The glaciers climate change initiative: Methods for creating glacier area, elevation change and velocity products," *Remote Sens. Environ.*, vol. 162, pp. 408–426, 2013.

[2] S. Wang, Y. He, and X. Song, "Impacts of climate warming on alpine glacier tourism and adaptive measures: A case study of baishui glacier no. 1 in yulong snow mountain, southwestern china," *J. Earth Sci.*, vol. 21, pp. 166–178, 2010.

[3] J. Gardelle, E. Berthier, and Y. Arnaud, "Slight mass gain of Karakoram glaciers in the early twenty-first century," *Nature Geosci.*, vol. 5, pp. 322–325, 2012.

[4] A. Kääb, "Combination of SRTM3 and repeat ASTER data for deriving alpine glacier flow velocities in the Bhutan Himalaya," *Remote Sens.d Environ.*, vol. 94, pp. 463–474, 2005.

[5] T. Bolch, T. Pieczonka, and D. I. Benn, "Multi-decadal mass loss of glaciers in the Everest area (Nepal Himalaya) derived from stereo imagery," *Cryosphere*, vol. 5, pp. 349–358, 2011.

[6] L. Ke, X. Ding, and C. Song, "Heterogeneous changes of glaciers over the western Kunlun Mountains based on ICESat and Landsat-8 derived glacier inventory," *Remote Sens. Environ.*, vol. 168, pp. 13–23, 2015.

[7] A. Kääb, E. Berthier, C. Nuth, J. Gardelle, and Y. Arnaud, "Contrasting patterns of early twenty-first-century glacier mass change in the Himalayas," *Nature*, vol. 488, pp. 495–498, 2012.

[8] J. Wei *et al.*, "Mass loss from glaciers in the chinese altai mountains between 1959 and 2008 revealed based on historical maps, SRTM, and ASTER images," *J. Mountain Sci.*, vol. 12, pp. 330–343, 2015.

[9] M. Willis, A. Melkonian, M. Pritchard, and A. Rivera, "Ice loss from the southern Patagonian ice field, South America, between 2000 and 2012," *Geophys. Res. Lett.*, vol. 39, L17501, 2012.

[10] Z. Li *et al.*, "Changes of climate, glaciers and runoff in China's monsoonal temperate glacier region during the last several decades," *Quaternary Int.*, vol. 218, pp. 13–28, 2010.

[11] Y. He, T. Yao, G. Cheng, and M. Yang, "Climatic records in a firn core from an Alpine temperate glacier on Mt. Yulong, southeastern part of the Tibetan Plateau," *Episodes*, vol. 24, pp. 13–18, 2001.

[12] M. Ren, Z. Liu, and W. Yong, "The preliminary study of the geomorphology in Yulong Mountain and Lijiang prefecture," *J. Yunnan Univ.*, vol. 4, pp. 9–18, 1957.

[13] Y. He, W. Theakstone, T. Yao, T. Chen, and D. Zhang, "The irregular pattern of isotopic and ionic signals in the typical monsoon temperate-glacier area, Yulong mountain, China," *Ann. Glaciol.*, vol. 35, pp. 167–174, 2002.

[14] Y. He, Z. Zhang, W. H. Theakstone, T. Chen, T. Yao, and H. Pang, "Changing features of the climate and glaciers in China's monsoonal temperate glacier region," *J. Geophys. Res. Atmospheres*, vol. 108, pp. 550–558, 2003.

[15] Y. He, "What is the major reason for glacier retreat on yulong mountain, China," *J. Glaciol.*, vol. 49, pp. 325–326, 2003.

[16] H. Pang, Y. He, W. H. Theakstone, and D. D. Zhang, "Soluble ionic and oxygen isotopic compositions of a shallow firn profile, Baishui glacier No. 1, southeastern Tibetan Plateau," *Ann. Glaciol.*, vol. 46, pp. 325–330, 2007.

[17] Z. Li *et al.*, "Chemistry of snow deposited during the summer monsoon and in the winter season at Baishui glacier No. 1, Yulong mountain, China," *J. Glaciol.*, vol. 55, pp. 221–228, 2009.

[18] H. Pang, Y. He, and N. Zhang, "Accelerating glacier retreat on Yulong Mountain, Tibetan Plateau, since the late 1990s," *J. Glaciol.*, vol. 53, pp. 317–319, 2007.

[19] Z. Li *et al.*, "Environmental significance of snowpit chemistry in the typical monsoonal temperate glacier region, Baishui glacier no. 1, Mt Yulong, China," *Environ. Geol.*, vol. 58, pp. 1319–1328, 2009.

[20] E. Berthier, Y. Arnaud, R. Kumar, S. Ahmad, P. Wagnon, and P. Chevallier, "Remote sensing estimates of glacier mass balances in the Himachal Pradesh (Western Himalaya, India)," *Remote Sens. Environ.*, vol. 108, pp. 327–338, 2007.

[21] A. Kääb, F. Paul, M. Maisch, M. Hoelzle, and W. Haeberli, "The new remote-sensing-derived Swiss glacier inventory: II. First results," *Ann. Glaciol.*, vol. 34, pp. 355–361, 2002.

[22] B. Song, "The applications of GIS and remote sensing technologies in Chinese temperate glacier areas," Ph.D. thesis, Cold Arid Regions Environ. Eng. Res. Inst., Chin. Acad. Sci., Beijing, China, 2008.

[23] J. K. Du *et al.*, "Response of modern monsoon temperate glacier to climate change in Yulong Mountain," *Scientia Geographica Sinica*, vol. 33, pp. 890–896, 2013.

[24] J. Du, Y. He, S. Li, S. Wang, and H. Niu, "Mass balance of a typical monsoonal temperate glacier in Hengduan Mountains Region," *Acta Geographica Sin.*, vol. 70, pp. 1415–1422, 2015.

[25] F. Paul, C. Huggel, and A. Kääb, "Combining satellite multispectral image data and a digital elevation model for mapping debris-covered glaciers," *Remote Sens. Environ.*, vol. 89, pp. 510–518, 2004.

[26] A. Racoviteanu, F. Paul, B. Raup, S. Khalsa, and R. Armstrong, "Challenges and recommendations in mapping of glacier parameters from space: results of the 2008 Global Land Ice Measurements from Space (GLIMS) workshop, Boulder, Colorado, USA," *Ann. Glaciol.*, vol. 50, pp. 53–69, 2010.

[27] A. Surazakov and V. Aizen, "Estimating volume change of mountain glaciers using SRTM and map-based topographic data," *IEEE Trans. Geosci. Remote Sens.*, vol. 44, no. 10, pp. 2991–2995, Oct. 2006.

[28] R. Bhambri, T. Bolch, and R. K. Chaujar, "Mapping of debris-covered glaciers in the Garhwal Himalayas using ASTER DEMs and thermal data," *Int. J. Remote Sens.*, vol. 32, pp. 8095–8119, 2011.

[29] B. Raup, A. Racoviteanu, S. J. S. Khalsa, C. Helm, R. Armstrong, and Y. Arnaud, "The GLIMS geospatial glacier database: A new tool for studying glacier change," *Global Planetary Change*, vol. 56, pp. 101–110, 2007.

[30] A. Kääb *et al.*, "Glacier mapping and monitoring using multispectral data," in *Global Land Ice Measurements From Space* (Springer Praxis Books). New York, NY, USA: Springer, 2014, pp. 75–112.

[31] Q. Cheng, H. Shen, L. Zhang, Q. Yuan, and C. Zeng, "Cloud removal for remotely sensed images by similar pixel replacement guided with a spatio-temporal MRF model," *ISPRS J. Photogrammetry Remote Sens.*, vol. 92, pp. 54–68, 2014.

[32] Q. Yuan, L. Zhang, and H. Shen, "Hyperspectral image denoising with a spatial–spectral view fusion strategy," *IEEE Trans. Geosci. Remote Sens.*, vol. 52, no. 5, pp. 2314–2325, May 2014.

[33] C. Woodcock *et al.*, "Free access to landsat imagery," *Science*, vol. 320, p. 1011, 2008.

[34] C. Zeng, H. Shen, and L. Zhang, "Recovering missing pixels for Landsat ETM + SLC-off imagery using multi-temporal regression analysis and a regularization method," *Remote Sens. Environ.*, vol. 131, pp. 182–194, 2013.

[35] T. Smith, B. Bookhagen, and F. Cannon, "Improving semi-automated glacier mapping with a multi-method approach: applications in central Asia," *Cryosphere*, vol. 9, pp. 1747–1759, 2015.

[36] A. Shukla, M. K. Arora, and R. P. Gupta, "Synergistic approach for mapping debris-covered glaciers using optical–thermal remote sensing data with inputs from geomorphometric parameters," *Remote Sens. Environ.*, vol. 114, pp. 1378–1387, 2010.

[37] J. L. Bamber and A. Rivera, "A review of remote sensing methods for glacier mass balance determination," *Global Planetary Change*, vol. 59, pp. 138–148, 2007.

[38] Z. Sun *et al.*, "Recent glacier dynamics in the northern novaya zemlya observed by multiple geodetic techniques," *IEEE J. Sel. Topics Appl. Earth Observ. Remote Sens.*, vol. 10, no. 4, pp. 1290–1302, Apr. 2017.

[39] E. Berthier, Y. Arnaud, C. Vincent, and F. Rémy, "Biases of SRTM in high-mountain areas: Implications for the monitoring of glacier volume changes," *Geophys. Res. Lett.*, vol. 33, L08502, 2006.

[40] C. Nuth and A. Kaab, "Co-registration and bias corrections of satellite elevation data sets for quantifying glacier thickness change," *Cryosphere*, vol. 5, pp. 271–290, 2011.

[41] J. Gardelle, E. Berthier, and Y. Arnaud, "Impact of resolution and radar penetration on glacier elevation changes computed from DEM differencing," *J. Glaciol.*, vol. 58, pp. 419–422, 2012.

[42] A. Dehecq, R. Millan, E. Berthier, N. Gourmelen, E. Trouvé, and V. Vionnet, "Elevation changes inferred from TanDEM-X Data over the mont-blanc area: Impact of the X-Band interferometric bias," *IEEE J. Sel. Topics Appl. Earth Observ. Remote Sens.*, vol. 9, no. 8, pp. 3870–3882, Aug. 2016.

[43] W. Guo *et al.*, "The second glacier inventory dataset of China (Version 1.0)," *Cold Arid Regions Sci. Data Center Lanzhou*, 2014.

[44] H. Xin, Y. He, and T. Zhang, "The features of climate variation and glacier response in Mt. Yulong, Southeastern Tibetan Plateau," *Adv. Earth Sci.*, vol. 28, pp. 1257–1268, 2013.

[45] A. Jarvis, H. I. Reuter, A. Nelson, and E. Guevara, "Hole-filled seamless SRTM data V4," Int. Centre Tropical Agriculture, Palmira, Colombia, 2008.

[46] P. Rosen, M. Eineder, B. Rabus, and E. Gurrola, "SRTM-Mission - cross comparison of X and C band data properties," in *Proc. Int. Geosci. Remote Sens. Symp.*, 2001, vol. 2, pp. 751–753.
[47] H. Frey and F. Paul, "On the suitability of the SRTM DEM and ASTER GDEM for the compilation of topographic parameters in glacier inventories," *Int. J. Appl. Earth Observ. Geoinf.*, vol. 18, pp. 480–490, 2012.
[48] L. Yue, H. Shen, L. Zhang, X. Zheng, F. Zhang, and Q. Yuan, "High-quality seamless DEM generation blending SRTM-1, ASTER GDEM v2 and ICESat/GLAS observations," *ISPRS J. Photogrammetry Remote Sens.*, vol. 123, pp. 20–34, 2017.
[49] P. Ramos and A. Serra, "A new sine-fitting algorithm for accurate amplitude and phase measurements in two channel acquisition systems," *Measurement*, vol. 41, pp. 135–143, 2008.
[50] K. Bhang, F. Schwartz, and A. Braun, "Verification of the vertical error in C-Band SRTM DEM Using ICESat and Landsat-7, Otter Tail County, MN," *IEEE Trans. Geosci. Remote Sens.*, vol. 45, no. 1, pp. 36–44, Jan. 2007.
[51] M. Shahgedanova, G. Nosenko, I. Bushueva, and M. Ivanov, "Changes in area and geodetic mass balance of small glaciers, Polar Urals, Russia, 1950-2008," *J. Glaciol.*, vol. 58, pp. 953–964, 2012.
[52] M. Lehning, H. Löwe, M. Ryser, and N. Raderschall, "Inhomogeneous precipitation distribution and snow transport in steep terrain," *Water Resources Res.*, vol. 44, 2008, Art. no. W07404.
[53] H. Machguth, O. Eisen, F. Paul, and M. Hoelzle, "Strong spatial variability of snow accumulation with helicopter-borne GPR on two adjacent Alpine glaciers," *Geophys. Res. Lett.*, vol. 33, pp. 338–345, 2006.
[54] K. Leonard and A. Fountain, "Map-based methods for estimating glacier equilibrium-line altitudes," *J. Glaciol.*, vol. 49, pp. 329–336, 2003.
[55] X. Liu, L. Bian, H. Lu, and Y. Zhu, "The accuracy assessment on slope algorithms with DEM error spatial autocorrelation," *Acta Geodaetica Et Cartographica Sin.*, vol. 37, pp. 200–206, 2008.
[56] P. A. Burrough, R. A. Mcdonnell, and C. D. Lloyd, *Principles of Geographical Information Systems*, vol. 12. London, U.K.: Oxford Univ. Press, 1998, pp. 102–102.
[57] A. Berg, G. Norgård, and G. Greve, "Annual temperature reconstruction in the Central Hengduan Mountains, China, as deduced from tree rings," *Dendrochronologia*, vol. 26, pp. 97–107, 2008.
[58] J. Du and Y. Ma, "Climatic trend of rainfall over tibetan plateau from 1971 to 2000," *Acta Geographica Sin.*, vol. 59, pp. 375–382, 2004.
[59] Y. Cai, D. Li, and Z. Bai, "Interdecadal variations of temperature and precipitation in Qinghai-Tibet plateau during the recent 50 years," *Highland Meteorol.*, vol. 22, pp. 464–470, 2003.
[60] J. Du, "The research of glacier change in the Yulong Snow Mountains based on RS and observation data," (in Chinese with English Abstract), master's thesis, Lanzhou Univ., Lanzhou, China, 2011.
[61] G. Zhang, Z. Li, W. Wang, and W. Wang, "Rapid decrease of observed mass balance in the Urumqi Glacier No. 1, Tianshan Mountains, central Asia," *Quaternary Int.*, vol. 349, pp. 135–141, 2014.
[62] L. Zhang *et al.*, "The 2010 spring drought reduced primary productivity in southwestern China," *Environ. Res. Lett.*, vol. 7, 2012, Art. no 045706.
[63] L. Liu, L. Jiang, Y. Sun, C. Yi, H. Wang, and H. Hsu, "Glacier elevation changes (2012–2016) of the Puruogangri ice field on the Tibetan Plateau derived from bi-temporal TanDEM-X InSAR data," *Int. J. Remote Sens.*, vol. 37, pp. 5687–5707, 2016.
[64] N. Neckel, A. Braun, J. Kropácek, and V. Hochschild, "Recent mass balance of the Purogangri Ice Cap, central Tibetan Plateau, by means of differential X-band SAR interferometry," *Cryosphere*, vol. 7, pp. 1623–1633, 2013.
[65] A. Rabatel *et al.*, "Can the snowline be used as an indicator of the equilibrium line and mass balance for glaciers in the outer tropics?," *J. Glaciol.*, vol. 58, pp. 1027–1036, 2012.
[66] B. Anderson *et al.*, "Climate sensitivity of a high-precipitation glacier in New Zealand," *J. Glaciol.*, vol. 56, pp. 114–128, 2010.

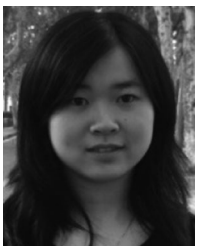

Linwei Yue received the B.S. degree in geographical information science and the Ph.D. degree in photogrammetry and remote sensing from Wuhan University, Wuhan, China, in 2012 and 2017, respectively.

In 2017, she joined the Faculty of Information Engineering, China University of Geosciences, Wuhan, China. Her research interests include terrain data processing, data fusion, and glacial environment monitoring.

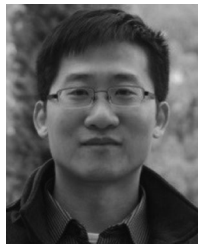

Huanfeng Shen (M'10–SM'13) received the B.S. degree in surveying and mapping engineering and the Ph.D. degree in photogrammetry and remote sensing from Wuhan University, Wuhan, China, in 2002 and 2007, respectively.

In July 2007, he joined the School of Resource and Environmental Sciences, Wuhan University, where he is currently a Luojia Distinguished Professor. His research interests include image quality improvement, remote sensing mapping and application, data fusion and assimilation, regional and global environmental change. He has published more than 100 research papers. He has been supported by several talent programs, such as The Youth Talent Support Program of China (2015), China National Science Fund for Excellent Young Scholars (2014), the New Century Excellent Talents by the Ministry of Education of China (2011).

Dr. Shen is currently a member of the Editorial Board of *Journal of Applied Remote Sensing*.

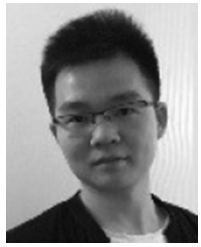

Wei Yu (M'13) received the B.S. degree in photogrammetry and remote sensing from Wuhan University, Wuhan, China.

He is currently a Data Engineer at AutoNavi Software Ltd., Alibaba Group, Beijing, China.

Liangpei Zhang (M'06–SM'08) received the B.S. degree in physics from Hunan Normal University, Changsha, China, in 1982, the M.S. degree in optics from the Xi'an Institute of Optics and Precision Mechanics, Chinese Academy of Sciences, Xi'an, China, in 1988, and the Ph.D. degree in photogrammetry and remote sensing from Wuhan University, Wuhan, China, in 1998.

He is currently the Head of the Remote Sensing Division, State Key Laboratory of Information Engineering in Surveying, Mapping, and Remote Sensing (LIESMARS), Wuhan University. He is also a "Chang-Jiang Scholar" Chair Professor appointed by the Ministry of Education of China. He is currently a Principal Scientist for the China state key basic research project (2011–2016) appointed by the Ministry of National Science and Technology of China to lead the remote sensing program in China. He has more than 450 research papers and 5 books. He is the holder of 15 patents. His research interests include hyperspectral remote sensing, high-resolution remote sensing, image processing, and artificial intelligence.